A multi-surface interface model for sequentially linear methods to analyse masonry structures

M. Pari [a,*], A.V. Van de Graaf [c], M.A.N. Hendriks [a,b], J.G. Rots [a]

[a] *Faculty of Civil Engineering and Geosciences, Delft University of Technology, P.O. Box 5048, Delft 2600 GA, The Netherlands*
[b] *Norwegian University of Science and Technology (NTNU), Rich. Birkelandsvei 1A, Trondheim 7491, Norway*
[c] *DIANA FEA B.V., Thijsseweg 11, Delft 2629 JA, The Netherlands*

ARTICLE INFO

ABSTRACT

In the finite element modelling of masonry structures, the micro-modelling technique of differentiating the continuum into a linear elastic bulk, and interfaces representing non-linear joints is common. However, this approach of simulating cracking-crushing-shearing failure possibilities in interfaces, typical of damage in masonry, also poses numerical stability issues due to the quasi-brittle nature of the failure. In this regard, the article proposes the use of numerically robust sequentially linear procedures and a suitable discretised tension-shear-compression failure model for interfaces. Sequentially linear solution procedures describe the nonlinear response of a specimen/structure through a sequence of scaled linear analyses, each of which represents locally applied damage increments, using secant-stiffness based discretised constitutive relations called saw-tooth laws. The constitutive formulation proposed herein includes a tension cut-off criterion combined with a uniaxial discretised softening law, a Coulomb friction criterion with a discretised cohesion softening law, and a compression cut-off criterion combined with a uniaxial discretised hardening–softening law. It is presented for both two-dimensional (2D) line interfaces and three-dimensional (3D) planar interfaces. The applicability of these formulations are illustrated using 2D and 3D models of a pushover analysis on a squat unreinforced masonry wall. The simulations are made using Sequentially Linear Analysis (SLA) and the Force-Release method, which are total (load-unload) and incremental sequentially linear methods respectively. The clear global softening in the force–displacement evolution and the localised brittle shear failure observed in the experiment are reproduced well and in a stable manner.

1. Introduction

Zero-thickness interface elements are used in standard Finite Element (FE) analysis to represent displacement discontinuities, for e.g. in plain and reinforced concrete applications to simulate cracking and bond slip failures. In masonry structures, global failure mechanisms generally comprise rocking, shear sliding and diagonal shear failures, or combinations thereof, which in turn involve a wide range of local mechanisms including cracking and slipping of joints, cracking under direct or diagonal tension of brick units, and masonry crushing at the toe of a rocking pier. Standard homogenised continuum representation of all such failure possibilities is possible [1] but at the expense of additional assumptions and is, furthermore, known to cause convergence issues in the traditional implicit nonlinear finite element analysis (NLFEA) setup. Alternatively, the micro-modelling strategy [2,3] has been employed by

differentiating the continuum into linear elastic bricks and potential failure planes represented by interface elements: along head and bed joints, and additionally, a potential vertical brick cracking plane. These non-linear failure planes allow for a discontinuous jump in the displacement field from one course of brick to the other or forming zigzag patterns which are characteristic of masonry failure. The commonly used constitutive framework in micro-modelling is the *composite-interface formulation* [4] under a traditional NLFEA set-up, which allows for combined cracking-crushing-shearing failures. Despite the simplification of modelling the nonlinearities into horizontal and vertical discrete interfaces, convergence issues in NLFEA persist due to the quasi-brittle nature of masonry failure [3,5,6], especially associated with the ultimate collapse which most often involves toe crushing.

Sequentially linear solution methods provide a numerically robust alternative for such explosive brittle failures. These secant-

---

stiffness–based event-by-event methods can be classified into three categories: purely *total* approaches [7–9] wherein unloading and reloading of all loads is done every step, purely *incremental* approaches [10–12] wherein the stress and loading history is explicitly tracked, and finally, a class of combined *incremental-total* approaches [12]. This article proposes a discretised tension-shear-compression failure model for interfaces, which is suitable to be used with sequentially linear methods such as Sequentially Linear Analysis (*total*) and the Force-Release method (*incremental*) for analysis of masonry structures. The novelty of the proposed constitutive model lies in allowing for tension–compression-shear failures in interfaces, in combination with non-proportional loading conditions in the sequentially linear framework, leading to automatic stable tracking of the post-peak response as in a structural collapse mechanism.

The article is organised as follows. Firstly, the sequentially linear analysis methodology is briefly described and reviewed in Section 2. Thereafter, the constitutive formulation for the two-dimensional (2D) line interfaces including the tension cut-off, Coulomb friction and compression cap criteria is detailed in Section 3.1, followed by the three-dimensional (3D) planar interface formulation in Section 3.2. Subsequently, the applicability of the formulations is illustrated using 2D and 3D models of a pushover analysis on a squat unreinforced masonry wall in Section 4. The simulations are made using both the Sequentially Linear Analysis (SLA) and Force-Release methods, thereby illustrating the applicability of the proposed failure criterion to sequentially linear methods in general.

2. Sequentially Linear Analysis (SLA): Methodology

Sequentially Linear Analysis (SLA) is a feature, as a part or whole, of several sequentially linear solution methods which have alternatively been referred to as non-iterative methods in literature [12]. Sequentially Linear Analysis (SLA) is a non-incremental (*total*) [13–15], secant stiffness-based event-by-event approach, wherein one linear analysis is performed at a time to identify and damage the *critical* integration point in the FE model. Therefore, it approximates the nonlinear response as a sequence of linear analyses with gradually increasing damage (damage-driven). The definition of the load multiplier per analysis step *j* for each integration point *i*, over all elements in the FE model, is shown below in a general sense, where f_i^j and $\sigma_{\text{gov},i}^j$ are the corresponding allowable strengths and the governing stresses respectively. The *critical* integration point is identified as the one with the minimum of all such positive load multipliers: the critical load multiplier λ_{crit}.

$$\lambda_i^j = \frac{f_i^j}{\sigma_{\text{gov},i}^j}, \quad \lambda_{\text{crit}}^j = \min_i\left(\lambda_{\text{crit},i}^j\right) \quad \forall \ \lambda_{\text{crit},i}^j > 0. \tag{1}$$

The linear analysis results i.e. displacements, forces, stresses and strains are then scaled using the critical load multiplier λ_{crit}. Subsequently, the strength and stiffness of this integration point are reduced in a step-wise manner based on a discretised constitutive relation, with successively reducing secant stiffnesses and allowable strengths, called the *saw-tooth law* (Fig. 1). This process of identifying critical events and load scaling is repeated until a user-defined stop criteria is reached or when the FE model is completely damaged. In summary, the method avoids multiple integration points being pushed simultaneously into failure, as in an incremental-iterative approach, and is therefore robust. In other words, SLA traces through every event, i.e. a jump or snap back, that may occur in the response of the structure. The combination of a *total* (load-unload) approach and the saw-tooth laws forms the crux of the method.

The approach has been under development from the early 2000s and is a proven alternative for applications in masonry [16], reinforced concrete [8] and glass [17]. Advancements in SLA include contributions to make the procedure mesh-objective [8,15]; saw-tooth laws for extremely brittle materials like glass (with snap-back at constitutive level) [17]; extensions to non-proportional loading situations [7][10]
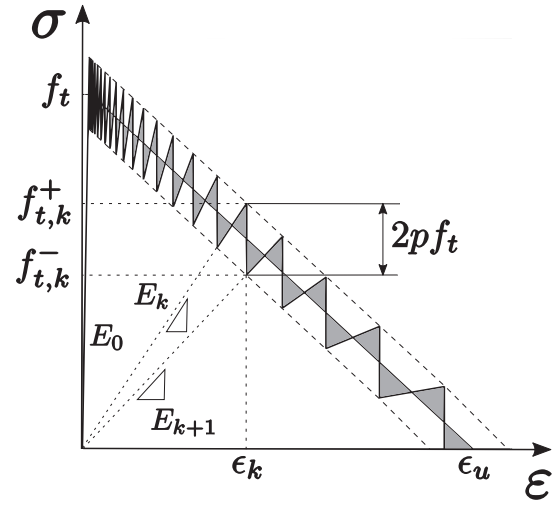

Fig. 1. Linear tension softening saw tooth law, with *p* the saw-teeth discretisation factor, based on the band width ripple approach to ensure mesh objectivity [15]. In this approach, a strength range *p* is defined as a percentage of the undamaged material strength f_t and a band is introduced into the softening part of the base curve, enclosing it such that the upper and lower triangles cancel each other out to eventually yield the same fracture energy.

[11][12][18][19]; extensions to interface elements with discrete cracking [20], bond-slip [21], and step-wise secant Coulomb friction laws [8]; creep induced cracking [22]; combined incremental-total approaches like Non-Iterative Energy based Method (NIEM) and the automatic method [12]; efficient linear solvers to improve the speed of SLA [23]; SLA in a stochastic setting [24]; combining SLA with crack tracking technique [25]; and mesh free SLA [26].

The aforementioned methodology was initially conceived for proportional loading conditions, and subsequently, modified for real loading schemes which often have multiple loads. The simplest and most common case is when there are constant loads on the structure like dead loads, precompression, overburden etc., and the structure is subsequently subject to variable loads like earthquake or wind or vehicle loads. Under such situations, the loading is considered to be non-proportional, and in the *total* approach of SLA, the system is loaded by constant loads (L_{con}) and a unit variable load (L_{var}). In case of the interfaces for example, the tractions are expressed as the superposition of the tractions due to the constant and scaled variable loads as shown in Eq. (2) for each integration point *i*. The governing stress is then limited by the allowable strengths *f*, corresponding to the failure criterion, as shown in Eq. (3), such that only the critical integration point *i* lies on the failure surface while all non-critical points lie below it. These equations apply for the normal direction (denoted by subscript *n* hereon), shear directions (denoted by subscripts *t* and *s* hereon) or combinations hereof (in case of frictional stress criteria). As long as Eq. (3) holds, Eq. (4) applies at the global level. Contrarily, when Eq. (3) fails in a certain analysis step *j*, the procedure is steered into the *Intermittent Proportional Loading* (denoted by subscript *ipl* hereon) [8], while implicitly reducing the constant load, as shown in Eq. (5) to reinstate Eq. (3). Such regions indicate the need for multiple failures representing a sudden propagation of damage.

$$t_i = t_{i,\text{con}} + \lambda \ t_{i,\text{var}} \tag{2}$$

$$\left(t_{i,\text{con}} + \lambda t_{i,\text{var}}\right) = f \ \wedge \ \forall i \ \neq \ k : \left(t_{k,\text{con}} + \lambda t_{k,\text{var}}\right) < f \tag{3}$$

$$L_{\text{crit}}^j = \lambda_{\text{con}} L_{\text{con}} + \lambda_{\text{var}} L_{\text{var}} \tag{4}$$

where $\lambda_{\text{con}} = 1$ and $\lambda_{\text{var}} = \lambda_{\text{crit}}$

$$L_{\text{ipl}} = L_{\text{con}} + \lambda_{\text{crit}}^{j-1} \ L_{\text{var}} \tag{5a}$$

$$L_{\text{ipl}}^{j} = \lambda_{\text{crit}}^{j}\, L_{\text{ipl}} \tag{5b}$$

Alternatively, in an *incremental* version like the Force-Release method [10], the non-proportional load path is discretised into a series of piece-wise proportional loading paths. Each prescribed load is discretised into a series of load vectors with magnitudes ensured to be non-decreasing, so that the proper loading/stress history is taken care of. Linear analyses are performed with load increments of a certain load vector, each of which may or may not lead to damage at a critical integration point i according to Eq. (6), wherein all quantities with Δ are the corresponding *incremental* values caused by the load increment. Upon damage, the stress from a damaged element is released gradually through a sequentially linear redistribution loop wherein the unbalanced forces due to the previous damage are applied as loads on the FE model, while all previously applied loads are kept constant, and other elements may be damaged. When the redistribution loop does not lead to further damage, the response stays in equilibrium. Otherwise, it evolves through states of disequilibrium and eventually returns to equilibrium. A comprehensive overview on the workflow of SLA and the Force-Release methods, and on the differences between such total and incremental sequentially linear methods for continuum applications can be found in Reference [27], and for lattice applications in References [10,28].

$$(t_i + \lambda \Delta t_i) = f \;\wedge\; \forall i \;\neq\; k: \; (t_k + \lambda \Delta t_k) < f \tag{6}$$

3. Constitutive model & workflow

A composite-interface formulation is proposed in this study, shown in Fig. 2, to be used in conjunction with the sequentially linear framework. The formulation is described hereon considering SLA as reference, although it applies to the Force-Release method as well. The tension-cut-off criterion is coupled with a uniaxial tension softening law. The compression-cap could be given an elliptical shape but is simplified herein as a cut-off criterion, dependent purely on the normal traction, coupled with a uniaxial hardening–softening law (referred to as the parabolic softening law [29,30] hereon). Step-wise secant saw-tooth laws address the aforementioned uniaxial material behavior. Finally, the Coulomb friction criterion which involves multiple stress and/or deformation components requires a more sophisticated approach for use in sequentially linear methods such as the SLA. In this regard, step-wise secant Coulomb friction laws proposed by Van de Graaf [8] for SLA are used herein. The sub-variant which decouples the tension and shear modes is the formulation considered in this study. Essentially, the dilatancy effects are neglected because of no coupling, i.e the dilatancy angle $\psi = 0$, an assumption that yields good results for masonry structures in general [2,31,32] and also using SLA [8]. Additionally, there exists a coupled sub-variant of the Coulomb friction model [8], wherein the update to the secant stiffness matrix $\mathbf{D}_{\text{sec}}$ is more complicated, but it is left out of the scope of this study.

In this section, both the 2D and 3D formulations are outlined for the different failure types in regard to the following aspects:

- Determination of the load multipliers per integration point in the FE model: $\lambda_i^{\text{shr}}, \lambda_i^{\text{ten}}$ and λ_i^{cmp} corresponding to the shear, tension and compression failures, and the identification of the critical integration point $\lambda_{\text{crit},i}$ and the corresponding failure mode.
- Updating the stiffness of the critical integration point based on the failure mode.

3.1. Line interfaces formulation (2D)

In the 2D interface formulation, at the linear elastic stage, the interface tractions t_n and t_t are related to the corresponding normal and shear relative displacements u_n[1] and u_t[1] by means of the uncoupled constitutive secant matrix $\mathbf{D}_{\text{sec}}$ (with an undamaged normal stiffness $k_{n,0}$ and shear stiffness $k_{t,0}$) in the following way.

$$\begin{bmatrix} t_n \\ t_t \end{bmatrix} = \begin{bmatrix} k_{n,0} & 0 \\ 0 & k_{t,0} \end{bmatrix} \begin{bmatrix} u_n \\ u_t \end{bmatrix} \tag{7}$$

3.1.1. Critical load multiplier

Shear mode. Considering initial cohesion c_0 and the yield criterion $|t_t| = -t_n\tan(\phi) + c_0$, the load multiplier for shearing failure per integration point i is defined as shown in Eq. (8), where $\tan(\phi)$ is the friction coefficient.

$$\left(|t_{t,i_{\text{con}}} + \lambda_i\, t_{t,i_{\text{var}}}|\right) + \left(t_{n,i_{\text{con}}} + \lambda_i\, t_{n,i_{\text{var}}}\right)\tan(\phi) \leqslant c_0 \tag{8}$$

Cohesion softening is considered for this study, and therefore the determination of the load multiplier per integration point is not equivalent to solving Eq. (8). This is because the mobilised cohesion c, in addition to being dependent on the plasticity parameter κ (assumed to be equal to the largest plastic relative shear displacement in the absolute sense [3]), becomes dependent on the load multiplier λ as shown in Eq. (9), where G_f^{II} is the mode-II fracture energy.

$$c(\kappa, \lambda) \;\; = c_0 \, \exp\left(-\frac{c_0}{G_f^{\text{II}}}\kappa\right)$$
$$\kappa \qquad = \max |u_t^{\text{pl}}| \tag{9}$$

Therefore, the load multiplier is deduced in the following way:

1. Evaluate load multipliers λ_{c_0} and λ_0, corresponding to states of initial cohesion and zero cohesion, as follows:

$$\left(|t_{t,i_{\text{con}}} + \lambda_{c_0}\, t_{t,i_{\text{var}}}|\right) + \left(t_{n,i_{\text{con}}} + \lambda_{c_0}\, t_{n,i_{\text{var}}}\right)\tan(\phi) \leqslant c_0 \tag{10a}$$

$$\left(|t_{t,i_{\text{con}}} + \lambda_0\, t_{t,i_{\text{var}}}|\right) + \left(t_{n,i_{\text{con}}} + \lambda_0\, t_{n,i_{\text{var}}}\right)\tan(\phi) \leqslant 0 \tag{10b}$$

2. Perform a bisection between λ_{c_0} and λ_0 to find an initial root, and then refine it using a Newton–Raphson scheme to arrive at the load multiplier λ_i^{shr} for shear failure, such that the integration point i lies on the shifted Coulomb surface (Fig. 2), i.e. the normalised yield lies below a user specified tolerance β as shown in Eq. (11).

$$\frac{\left(|t_{t,i_{\text{con}}} + \lambda_i^{\text{shr}}\, t_{t,i_{\text{var}}}|\right) + \left(t_{n,i_{\text{con}}} + \lambda_i^{\text{shr}}\, t_{n,i_{\text{var}}}\right)\tan(\phi) - c}{c_0} \leqslant \beta \tag{11}$$

The friction coefficient is assumed to be constant i.e. friction softening is neglected. Note that in case the cohesion softening is absent, λ_i^{shr} can be calculated according to Eq. (10a).

Tension mode. The load multiplier for tensile cracking is as shown in Eq. (12), where f_t is the current tensile strength based on a predefined saw-tooth law (Fig. 1), or on a stress–strain relation evolving during analysis with *user-specified* relative displacement increments and the corresponding traction decrements [8], as shown in Fig. 3(a).

$$\left(t_{n,i_{\text{con}}} + \lambda_i^{\text{ten}}\, t_{n,i_{\text{var}}}\right) \leqslant f_t \tag{12}$$

---

[1] The Δ symbol, commonly used to denote *relative* displacements in interface formulations, is dropped herein to avoid ambiguity with the variations of the said relative displacements used in the *stiffness update* subsection
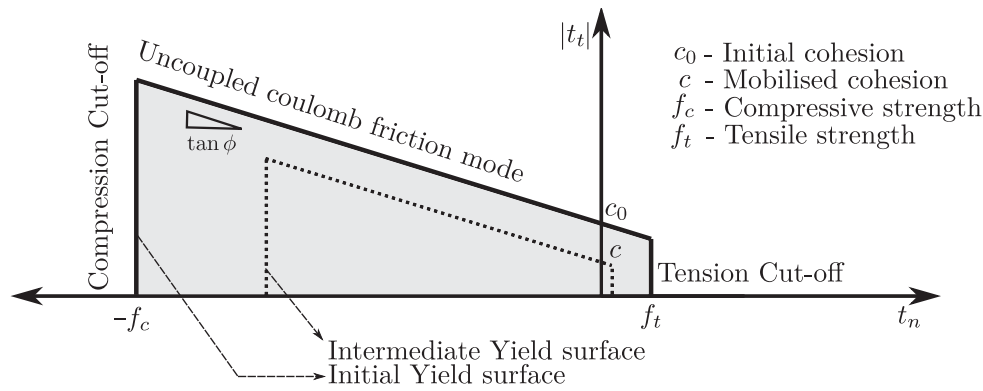
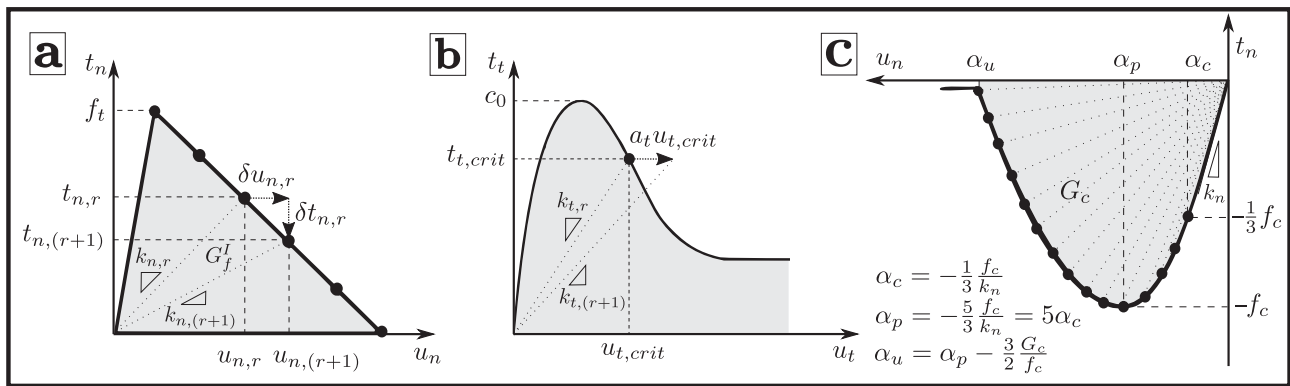**Fig. 2.** Failure surface for the 2D line interfaces.

Fig. 3. (a) Linear tension softening law evolving 'during' analysis with user specified relative normal displacement increments, (b) cohesion softening law deduced 'during' analysis with user specified relative shear displacement increments, and (c) pre-defined parabolic hardening–softening saw-tooth law for compression [29]. Studies in this article use (b) as such for the shear mode, while predefined band width ripple versions of (a)&(c) (Fig. 1) are used for tension and compression.

Compression mode. The load multiplier for crushing failure is as shown in Eq. (13), where f_c is the current compressive strength based on a predefined parabolic softening saw-tooth law as shown in Fig. 3(c). The failure criterion for compression in the original composite interface formulation for masonry [3] is an ellipsoid cap model that depends on the normal and shear stresses through a set of material parameters. However, for simplicity, this is herein treated as a straight shear-independent cut-off criterion. This approach is reasonably accurate and also fits well with material parameters such as the compressive strength f_c and fracture energy G_c, which are widely used in engineering practice for e.g. in a simple Rankine-type failure surface for the total strain–based smeared cracking models.

$$\left(t_{n,i_{\mathrm{con}}} + \lambda_i^{\mathrm{cmp}}\, t_{n,i_{\mathrm{var}}}\right) \geqslant -f_c \tag{13}$$

The critical load multiplier is then determined as the minimum of all the load multipliers.

$$\lambda_{\mathrm{crit}} = \min_i\left(\lambda_i^{\mathrm{shr}}, \lambda_i^{\mathrm{ten}}, \lambda_i^{\mathrm{cmp}}\right) \tag{14}$$

3.1.2. Stiffness update

Once the critical integration point is identified, the stiffness matrix is degraded based on the failure mode as detailed in the following.

Shear mode. The shear failure involves update to *only* the shear stiffness term of the uncoupled constitutive matrix $\mathbf{D}_{\mathrm{sec}}$, which is defined for the jth linear analysis or step as follows

$$\mathbf{D}_{\mathrm{sec}}^{(j)} = \begin{bmatrix} k_n^{(j)} & 0 \\ 0 & k_t^{(j)} \end{bmatrix} \tag{15}$$

$$k_t^{(j)} = \frac{t_{t,\mathrm{crit}}^{(j-1)}}{u_{t,\mathrm{crit}}^{(j-1)} + \delta u_t^{(j-1)}} \quad \text{with } \delta u_t^{(j-1)} = a_t u_{t,\mathrm{crit}}^{(j-1)} \tag{16}$$

The update to the shear stiffness is computed during the analysis, as shown in Eq. (16), with the critical shear traction $t_{t,\mathrm{crit}}^{(j-1)}$ and the critical relative shear displacement $u_{t,\mathrm{crit}}^{(j-1)}$ of the completed $(j-1)^{\mathrm{th}}$ step, and additionally, a specified relative shear displacement increment $\delta u_t^{(j-1)}$ which is based on a user defined factor a_t. This factor is similar to the saw-tooth band width ripple factor p, as in Fig. 1, and is used for discretising the constitutive behavior. The updated shear stiffness $k_t^{(j)}$ therefore corresponds to the increased shear displacement $(1 + a_t)u_{t,\mathrm{crit}}^{(j-1)}$, and is a prediction that is exact *only* if the actual shear displacement in the subsequent step will equal the specified increased shear displacement. This way of updating stiffness during an ongoing analysis is merely an alternative approach to the a priori definition of saw-tooth laws. This is also shown in the cohesion softening law evolving during analysis in Fig. 3(b), wherein subscripts *r* for the shear stiffness k_t refer to the subsequent saw teeth number in the softening law (not to be confused with analysis step *j*). The effect of larger values of the user defined factor a_t was previously shown to result in a saw-tooth (coarser) type response in the force displacement evolution, due to the approximate stiffness guess, for a shear study on bricks under confinement [8].

Tension and Compression modes. Both the cracking and crushing failures consider the normal traction for damage initiation and propagation. Accordingly, both failures involve update to the normal stiffness term of the uncoupled constitutive matrix $\mathbf{D}_{\mathrm{sec}}$, shown in Eq. (15), based on predefined saw-tooth laws. For tensile cracking, linear tension

softening relations are approximated as the predefined band width ripple type saw-tooth law shown in Fig. 1. Alternatively, similar to the cohesion softening law evolving during analysis, the normal stiffness updates can be made on the basis of a specified normal relative displacement increment $\delta u_{n,r}$ and an associated drop in normal traction $\delta t_{n,r}$ for the current saw-teeth number r as shown in Fig. 3(a). For compressive failures, the band width ripple version of the parabolic hardening–softening relation shown in Fig. 3(c) is used.

Furthermore, the shear stiffness is also damaged in both cases as shown in Eq. (17), where $k_{n,0}$ and $k_{t,0}$ are the undamaged normal and shear stiffnesses. However, if the current shear stiffness $k_t^{(j-1)}$ at the end of the completed analysis step $(j-1)$ is lesser than the computed $k_t^{(j)}$, the shear stiffness is not degraded any further.

$$k_t^{(j)} = k_{t,0} \frac{k_n^{(j)}}{k_{n,0}} \tag{17}$$

The original composite interface model [3] was plasticity-based, i.e. with elastic unloading/reloading. In contrast, the proposed model has secant unloading/reloading for all modes. This better fits quasi-brittle materials particularly in relation to discrete cracking. This is because elastic unloading of fully open tensile cracks, as in the original formulation, could result in an overly-stiff behaviour which is not desirable. In this sense, the proposed model is advantageous. However, the use of a total approach may result in inappropriate crack-closure effects under redistribution, with carry over of damaged stiffness between stress regimes.

3.2. Planar interfaces formulation (3D)

The composite failure surface being proposed for planar (3D) interfaces is shown in Fig. 4. In the 3D interface formulation, at the linear elastic stage, the interface tractions t_n, t_t and t_s are related to the corresponding normal and shear relative displacements u_n, u_t and u_s respectively by means of the uncoupled constitutive secant matrix $\mathbf{D}_{sec}$ (with undamaged normal stiffness $k_{n,0}$ and shear stiffnesses $k_{t,0}$ & $k_{s,0}$) in the following way.

$$\begin{bmatrix} t_n \\ t_t \\ t_s \end{bmatrix} = \begin{bmatrix} k_{n,0} & 0 & 0 \\ 0 & k_{t,0} & 0 \\ 0 & 0 & k_{s,0} \end{bmatrix} \begin{bmatrix} u_n \\ u_t \\ u_s \end{bmatrix} \tag{18}$$

3.2.1. Critical load multiplier

The load multiplier definition for the tension and compression failure modes for the 3D planar interfaces are the same as those for the 2D case, as shown in Eq. (12) and (13), since the cracking or crushing initiation and propagation depends on the normal traction t_n. However, with regard to the shear failure mode in planar interfaces, the yield criterion for

an integration point i is governed by the effective shear stress [33] which is defined as follows.

$$
\begin{aligned}
t_{eff,i} &= -t_{n,i}\tan(\phi) + c_0 \\
\text{where} \quad t_{eff,i} &= \sqrt{t_{t,i}^2 + t_{s,i}^2}
\end{aligned} \tag{19}
$$

Accordingly, the plasticity parameter κ is also expressed as the effective plastic shear relative displacement in the following manner.

$$u_{t,eff}^{pl} = \sqrt{u_t^{pl2} + u_s^{pl2}} \tag{20}$$

Rest of the workflow to determine the load multiplier for shear failure is similar to the 2D formulation, wherein equations Eqs. (8)–(11) hold with the appropriate effective shear stress and the effective plastic shear relative displacement. The critical load multiplier is then deduced according to Eq. (14), and the stiffness update for the corresponding failure mode is carried out as explained in the following subsection.

3.2.2. Stiffness update

Shear mode. Similar to the 2D formulation, the shear failure involves update to the shear stiffness terms of the 3D uncoupled constitutive matrix $\mathbf{D}_{sec}$ in Eq. (21). Both the shear stiffnesses are calculated based on user-specified relative shear displacement increments $\delta u_t^{(j-1)}$ and $\delta u_s^{(j-1)}$, which now require two user defined factors a_t and a_s, during an ongoing analysis step j as shown in Eq. (22).

$$\mathbf{D}_{sec}^{(j)} = \begin{bmatrix} k_n^{(j)} & 0 & 0 \\ 0 & k_t^{(j)} & 0 \\ 0 & 0 & k_s^{(j)} \end{bmatrix} \tag{21}$$

$$
\begin{aligned}
k_t^{(j)} &= \frac{t_{t,crit}^{(j-1)}}{u_{t,crit}^{(j-1)} + \delta u_t^{(j-1)}} \quad \text{with} \quad \delta u_t^{(j-1)} = a_t u_{t,crit}^{(j-1)} \\
k_s^{(j)} &= \frac{t_{s,crit}^{(j-1)}}{u_{s,crit}^{(j-1)} + \delta u_s^{(j-1)}} \quad \text{with} \quad \delta u_s^{(j-1)} = a_s u_{s,crit}^{(j-1)}
\end{aligned} \tag{22}
$$

Tension and Compression modes. The update to the normal stiffness in case of cracking and crushing failures, involves resorting to the predefined or evolving tension and compression softening saw-teeth relations, again similar to the 2D formulation. However, in addition to the update to normal stiffness, the shear stiffness is damaged along both shear directions as shown in Eq. (23), unless the current shear stiffnesses $k_t^{(j-1)}$ and $k_s^{(j-1)}$ at the end of the completed analysis step $(j-1)$ are lesser than the newly computed $k_t^{(j)}$ and $k_s^{(j)}$.
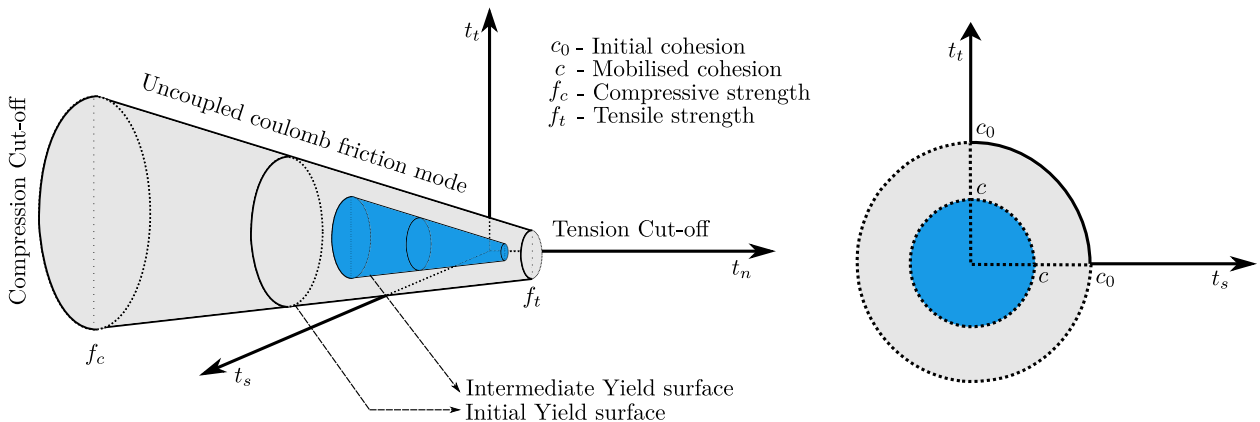

Fig. 4. Failure surface for the 3D planar interfaces.

$$k_t^{(j)} = k_{t,0} \frac{k_n^{(j)}}{k_{n,0}}$$

$$k_s^{(j)} = k_{s,0} \frac{k_n^{(j)}}{k_{n,0}}$$

(23)

4. Illustration: Pushover analysis of a masonry wall

Experiment. In this section, the experiment on a solid clay brick masonry wall tested by Raijmakers and Vermeltfoort [34,35] is used as a benchmark to validate the proposed 2D and 3D composite interface formulations. The wall was made of 18 courses of bricks, with dimensions of 210 mm × 52 mm × 100 mm, and mortar layers of 10 mm thickness. The dimensions of the wall are as shown in Fig. 5(a), based on the 18 courses of bricks, resulting in an approximate effective width/height ratio of one. The top and bottom courses of bricks were clamped to a steel beam to constrain the rotation along both edges, additionally preventing the free vertical movement of the top edge. The walls were loaded initially by an overburden pressure of 0.30 N/mm$^2 \triangleq 30$ kN, followed by a monotonically increasing lateral load d applied under displacement control. The damage patterns of two such walls, namely J4D and J5D, are shown in Figs. 5(b), (c). The damage in both walls begins with a rocking type failure i.e. cracks developing along the top and bottom of the wall. This is followed by a diagonal stepped crack which leads to the failure mechanism, simultaneously with cracks in the bricks and crushing of the compressed toes of the wall. Such a mechanism and the availability of data on material properties, including fracture energies from small-scale companion tests, makes this an ideal benchmark considering the scope of the proposed composite interface formulations.

4.1. 2D Line interface micro-model

Finite Element Model. The walls are discretised using the simplified micro-modelling strategy [2,3], wherein mortar joints and the brick–mortar interfaces are lumped together into a zero-thickness interface, and the bricks are extended to account for the mortar thickness. The bricks are modelled using 4-noded iso-parametric plane stress elements, roughly 27.5 mm × 27.5 mm in size, with linear interpolation shape functions and a 2×2 Gaussian integration scheme. The zero-thickness interfaces are modelled using $2 + 2$ noded interface elements, allowing for 2 in-plane translational degrees of freedom (DOFs) per node, in conjunction with a 2-point Newton–Cotes integration scheme. All DOFs along the bottom edge of the wall are fully constrained, while the top edge is prevented against any rotation. The nodes along the top edge of the wall are given an initial vertical displacement

0.083 mm, which is the imposed displacement equivalent to an overburden pressure of 0.30 N/mm^2. Subsequently, a lateral displacement is imposed on the top edge to simulate the lateral load.

The FE model shown in Fig. 6 includes interfaces along the head and bed joints, and additionally, along the mid-length of bricks to simulate vertical brick cracks. The 2D composite line interface formulation is the adopted constitutive model, and all head and bed joints are lumped with the nonlinearities of tensile cracking, crushing and shearing, with material parameters as shown in Tables 1,2. The predefined band width ripple based linear tension softening and parabolic compression hardening–softening saw-tooth laws are used. The properties for compression are reduced in comparison to those used in Reference [3], by means of a sensitivity study, to fit the experimental results. This is also motivated by the use of a straight cap (cut-off) criterion instead of the elliptical cap for compression failure. For the decoupled Coulomb friction failure mode, a user specified discretisation factor of $a_t = 0.05$ for the specified relative shear displacement, as in Eq. (16), is used. The
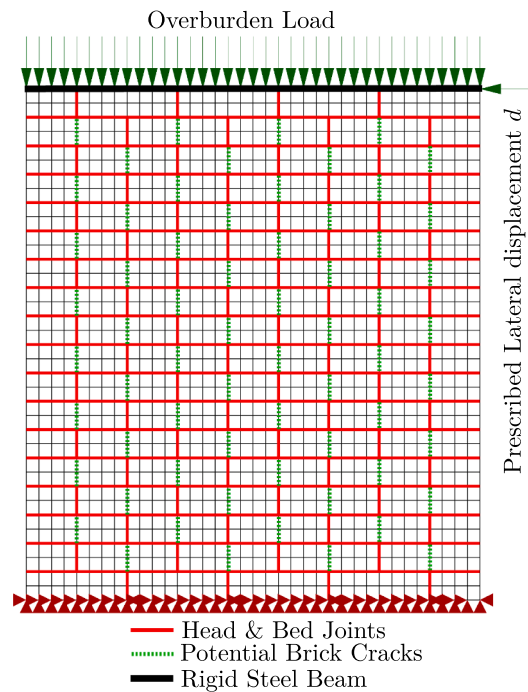

Fig. 6. 2D Finite element micro model of the solid clay brick wall subject to overburden and pushover loads.
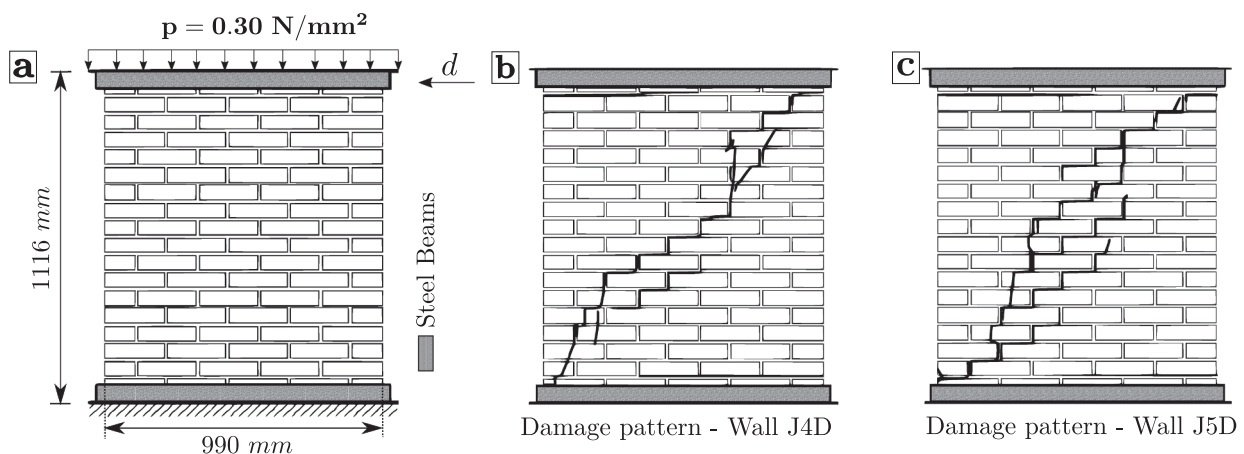

Fig. 5. (a) Schematic representation of solids clay brick masonry walls (J4D & J5D), loaded firstly by an overburden pressure of 0.30 N/mm^2 followed by a lateral prescribed displacement d; and the experimental crack patterns of the walls (b) J4D and (c) J5D.

Table 1

Elastic modelling parameters – J4D and J5D walls: based on References [34,35,3].

Masonry Units	Parameters	Elastic
Bricks	Young's Modulus E_0 [GPa]	16.7
	Poisson's ratio v_0	0.15
Head & Bed Joints	Normal stiffness k_n [N/mm³]	82
	Shear stiffness k_t [N/mm³]	36
Brick Cracks	Normal stiffness k_n [N/mm³]	10^6
	Shear stiffness k_t [N/mm³]	10^6

Table 2

Inelastic modelling parameters based on References [34,35,3] (except compression).

Masonry Units	Parameters	Compression	Tension	Shear
Head & Bed Joints	Strength f_t, f_c, c_0 [MPa]	6.0	0.25	0.35
	Fracture energy G_c, G_f^I, G_f^{II} [N/mm]	1.8	0.018	0.125
	Saw-teeth discretisation factor	0.1	0.15	0.05
	Softening relation Shear retention factor β	Parabolic Damage-based [36]	Linear Damage-based [36]	Exponential –
Bricks Cracks	Tensile Strength f_t [MPa]		2	
	Fracture energy G_f^I [N/mm]		0.08	
	Saw-teeth discretisation factor		0.2	
	Softening relation Shear retention factor β		Linear Damage-based [36]	

factor describes the shear displacement increments per linear analysis for the critical integration point, and this is chosen as 0.05 based on the previous study of the same specimen [8]. Higher values may result in quicker loss of mobilised cohesion and lower dissipation of shear fracture energy, and therefore are not used. Vertical interfaces are included in the middle of the bricks, with only the discrete cracking possibility while omitting the shear and compression failures, in accordance to previous studies in References [4,8]. Additionally, the overall brick behaviour and the vertical brick crack joints along the bottom and topmost course of bricks in particular, which are attached to the stiff steel beams, are kept linear elastic with material parameters as shown in Table 1.

4.1.1. Results & discussion

Firstly, the performance of the micro-model with the full composite interface formulation, i.e. discrete cracking, shearing and crushing in the interfaces, is analysed. This is treated as the reference case and is referred to as the *discrete-crushing* model hereon. The force–displacement evolution for this pushover study, shown in Fig. 7, shows good qualitative agreement with the experimental responses of walls J4D and J5D, in terms of the peak loads, and the global softening behaviour that leads to loss of lateral capacity. The deformed profile and damage propagation in the masonry are summarised for the SLA simulation of this model in Fig. 8, at 2 mm and 4 mm prescribed lateral top displacements. The damage plots DmTeNN and DmCoNN indicate loss of normal stiffness due to cracking and crushing respectively. The DmTeSS damage plots indicate loss of shear stiffness which is either due to a pure-
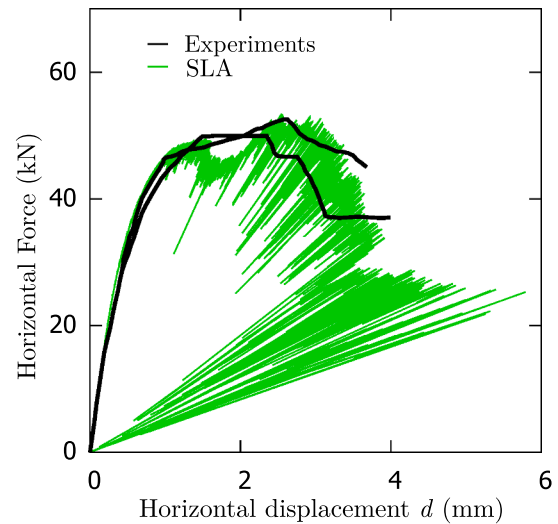

Fig. 7. Force–displacement curves of the experiments compared against those of SLA for the reference micro model with discrete cracking, shearing and crushing in interfaces.
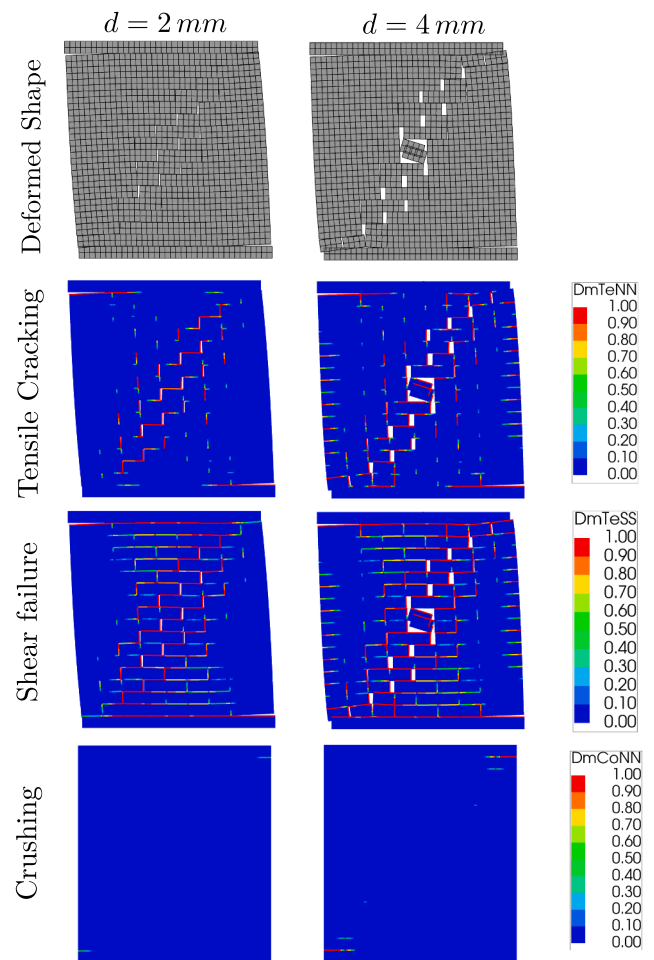

Fig. 8. The deformed profile, and damage plots indicating tensile, shear and crushing failures for the pushover study of reference *discrete-crushing* model, with discrete cracking-shearing-crushing interfaces, using SLA at 2 mm and 4 mm prescribed lateral displacements.

sliding failure or the damage based shear reduction associated with the cracking/crushing modes. All damage plots herein range from 0 to 1 which refer to undamaged and fully damaged cases for the corresponding failure criteria.

The wall firstly exhibits flexural failure which is visible as horizontal cracks along bed joints at the bottom-right and top-left corners of the wall. After the flexural cracks are fully developed (before 2 mm top displacement), compressive strut action results in a staggered step-like crack along the diagonal to the toe (left bottom corner) of the wall. This damage propagation includes both sliding failure along the bed joints, resulting in loss of shear stiffness, and tensile cracking along head joints, resulting in loss of both normal and shear stiffnesses. The fully developed flexural cracks and propagating diagonal step cracks at 2 mm top displacement are shown as tensile cracking and shear failure plots in Fig. 8. Furthermore, the stress flow into the toe of the wall leads to the onset of the crushing failure, which can be seen as loss of normal stiffness in the crushing plots of Fig. 8.

Upon further increase of the lateral displacement to 4 mm, the damage along the diagonal shear crack increases and localises, leading to a widening of the head joints and simultaneous sliding along bed joints, along the diagonal of the wall. Furthermore, the stepped crack also involves vertical splitting cracks through the bricks along the courses at mid-height of the wall, which often appear as sudden drops/ instabilities in traditional NLFEA [3]. This is adequately captured by SLA. Simultaneously, the toe of the wall is completely crushed along half the length of an entire brick. This results in a clear drop of lateral capacity which is observed in the force–displacement curve, indicating structural collapse.

The performance of the model can also be assessed based on the development of the vertical reaction forces, and its eccentricity with respect to the center line of the wall. The comparison of these aspects with the experiments is shown in Fig. 9. Firstly, the general trend of the increase in vertical reaction with increasing lateral displacement is captured reasonably well. However, the results are adrift of the experiment. Secondly, the development of eccentricity (x/w) of the effective vertical reaction, where w is half the width of the wall and x is the distance of the effect vertical reaction force from the center line of the wall, is analysed. The eccentricity first grows outwards and eventually inwards to the center line of the wall with increasing lateral displacement in the SLA simulation. This is similar to the trends from the experiments, however, once again differences are observed. Despite the two above mentioned artefacts, the force–displacement evolution seems to be captured perfectly and therefore, these are considered acceptable in this study. Furthermore, despite the assumption of zero dilatancy

angle, which is a feature of the decoupled Coulomb friction model used herein, the force–displacement response is close to the experiment. This is in line with the findings of previous works [2,31,32] on the acceptable use of zero-dilatancy angle in the analysis of masonry structures. Finally, the performance of the non-proportional loading strategy in SLA in fully retaining the constant load until physical failure is remarkable in this case, and this is discussed in detail the following section.

4.1.2. Variation studies

The following variations are performed on the benchmark study to analyse the performance of the proposed composite interface formulation.

- Firstly, the micro-model is run with discrete cracking and shearing failure possibilities in the interfaces excluding compressive nonlinearities, to understand the influence of crushing that is often the primary cause of collapse in masonry units such as shear walls. This case is referred to as the *no-crushing* model hereon.
- Secondly, the reference micro-model with full composite interface failure possibilities, i.e. the *discrete-crushing* model previously analysed using the SLA, is additionally studied using an incremental sequentially linear method called the Force-Release method. This helps to understand the influence of non-proportional loading in SLA, and also the importance of tracking stress history on damage accumulation and the eventual failure mechanism.
- Thirdly, a variation is performed with a micro model which distinguishes only the cracking and shearing failures into the interfaces. The crushing is smeared into the continuum brick elements using an orthogonal fixed smeared crush model. This case is referred to as the *smeared-crushing* model hereon.

Case 1: Influence of crushing. The force displacement curves of the *no-crushing* model compared against the reference *discrete-crushing* model is shown in Fig. 10. The importance of crushing nonlinearities is clearly observed in the response of the *no-crushing* model which shows progressive increase in capacity with an increasing prescribed lateral displacement. This is also confirmed by the growing compressive tractions, in the bed joint interface near the toe of the wall, to almost 20 MPa at 4 mm top displacement as seen in Fig. 11. Contrarily, the response of the reference *discrete-crushing* model shows a nonlinear distribution of compressive tractions along the length of the said bed joints already at 2 mm top displacement. With further increase in lateral displacement, the tractions in the bed joints drop and move inwards towards the center of the wall. This indicates crushing of the toe. Fig. 11 shows the formation
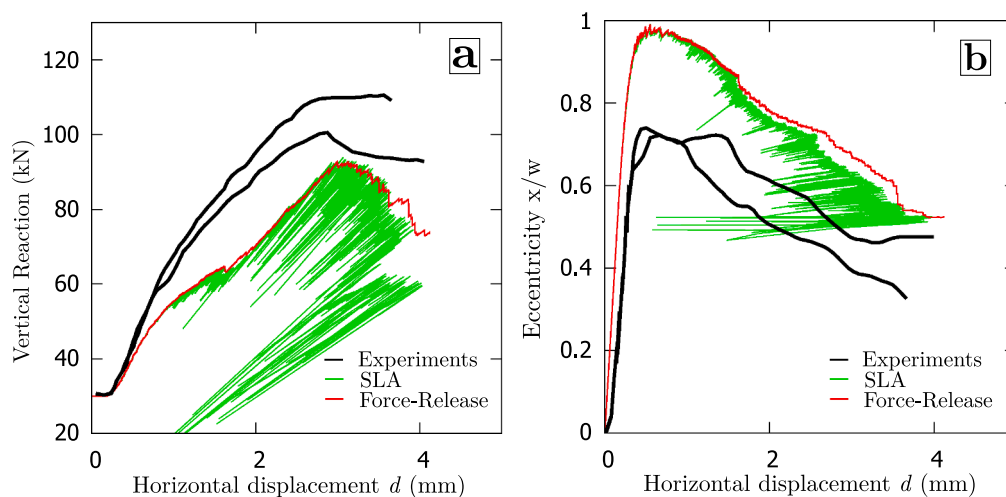

Fig. 9. (a) Evolution of the vertical reaction forces and (b) its eccentricity with respect to the center line of the wall, for increasing prescribed lateral displacements in the SLA and Force-Release simulations (discussed under Case-2 of the section on variation studies) of the *discrete-crushing* model.
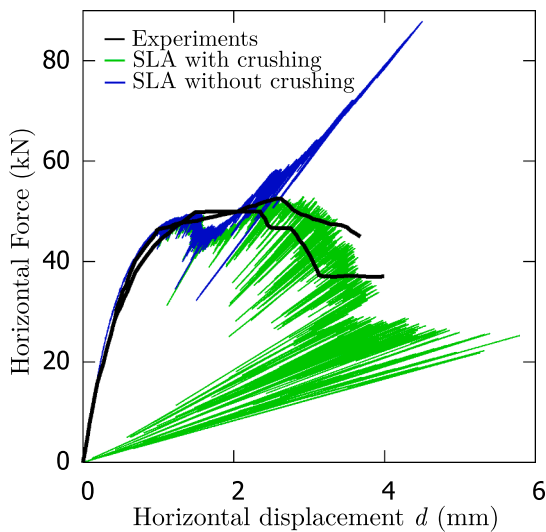
Fig. 10. Force–displacement curves of the SLA simulation of the micro models with and without crushing nonlinearities.
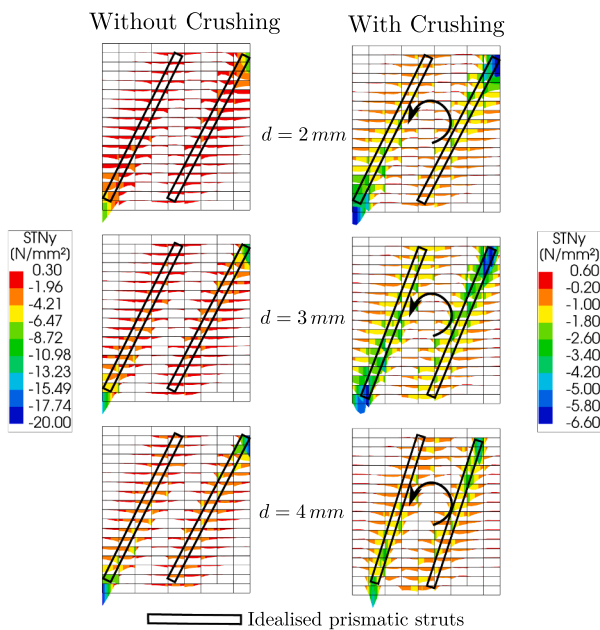

Fig. 11. Evolution of compressive tractions along bed joints of the wall, with and without the crushing failure possibility (note the different colour scales), for increasing lateral displacements and the schematic view of the rotation and movement of two parallel struts in the case of crushing failure possibility, with progressive crushing of the toe region of the wall.

of two parallel struts which are both rotating and approaching each other, which is also exemplified by the variation of eccentricity of the effective vertical force in Fig. 9(b). This study validates the proposed simplified cut-off criterion used for crushing in the composite interface formulation. Although an elliptical cap model is used in the original formulation [3], the simplified straight cap (cut-off) criterion, in conjunction with other assumptions for the shear formulation and calibrated properties in compression, performs remarkably well.

Case 2: SLA vs Force Release method. A Force-Release simulation of the reference *discrete-crushing* model is performed to check the validity of the composite interface formulation for incremental sequentially linear methods. The force displacement curve for the Force-Release simulation of the pushover study is as shown in Fig. 12(a). It compares well with

SLA and is mostly an envelope of the SLA response. This is corroborated by the close similarity in the damage plots of the SLA and Force-Release simulations at 2 mm prescribed lateral displacement, refer Figs. 8 and 13.

The differences become apparent whenever SLA returns to the *Intermittent Proportional Loading* (IPL), wherein the last successful load combination is scaled proportionally to avoid violation of the constitutive law anywhere in the FE model. Under such conditions, the overburden load in SLA is implicitly reduced to enforce equilibrium during a quasi-static damage driven failure propagation. This becomes significant starting $\sim$ 3.7 mm prescribed lateral displacement, marked as a yellow circle in Fig. 12, indicating onset of collapse. The constant load drops to extremely low values through this region but is also recovered immediately (Fig. 12(b)), which appears as large snap-backs in the post-collapse region at prescribed lateral displacements around 4 mm. Since every damaged element's stress is released instantaneously in SLA, the neighbouring integration points of the critical integration point whose stresses are close to their respective allowable strengths subsequently become critical at a considerably lower load. In summary, the performance of the non-proportional loading strategy of SLA is successful in this problem leading to collapse, which in turn is described using its inherent redistribution procedure i.e. the IPL.

On the other hand, these regions are simulated in disequilibrium using the Force-Release method appearing as instabilities or *drops* of load for a constant imposed displacement. The collapse mechanism herein is captured by both approaches adequately. However, the drop of load corresponding to the eventual instability is described by the SLA and the Force-Release methods in diametrically opposite ways, with regard to the time scales for the redistribution. This is in line with the differences observed between the approaches to typical explosive failure in the previous case studies [27], and is clear from how the loading is modified in case of SLA (Fig. 12(b)) during collapse. SLA describes the entire collapse while maintaining equilibrium by reducing the constant load, while the Force-Release method addresses it using the avalanche of damage states in disequilibrium which appear as vertical drops of the capacity. Furthermore, it is known that the difference in load history between SLA and the Force-Release method results in a different elemental failure sequence in lattice simulations [10], and that for continuum studies as well damage propagation could be different, by a small amount, which was confirmed by a previous study [27]. This is reiterated by the current case study as well which is evident from damage plots for SLA and Force-Release at 4 mm top displacement, refer Figs. 8 and 13. Although the plots look alike, there are yet notable differences like the through vertical cracks in the middle course of bricks in SLA which appears to be more like a stepped crack passing through the head and bed joint in the Force-Release case. Furthermore, the failure is more localised in case of SLA. Such minor differences are the effect of an accumulation of differences in damage locations over several steps. The IPL is used in SLA often after 50000 events as seen in Fig. 12(b), while the Force-Release traverses through these regions through several small instabilities. Another prominent region is around 4.25 mm prescribed lateral displacement of both SLA and Force-Release curves in Fig. 12(a). Furthermore, the evolution of vertical reaction forces and its eccentricity with the imposed displacement in the Force-Release simulation is also similar to that of SLA, refer Fig. 9. In conclusion, Force-Release simulation (*incremental*) of the composite interface formulation also performs well for the case study and compares well with the *total* version of SLA.

The suitability of the two methods depends on the type of experiment being simulated. Force-Release method is suitable for typical displacement controlled experiments which actually exhibit instabilities. These would be consistent with the drops of loads observed in Force-Release simulations. On the other hand, it may not be suitable for physical processes which exhibit snap backs or for truly quasi-static experiments. SLA is more preferable when the damage process zone is unique and controlled for quasi-static evolution in an experiment [37]. However, for a Crack Mouth Opening Displacement (CMOD) controlled experiment
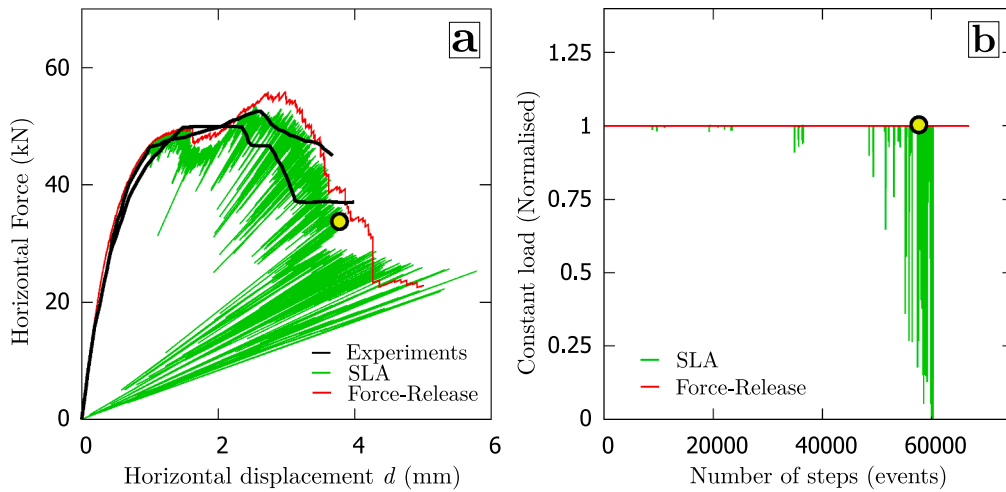
Fig. 12. Force–displacement curves of the experiments compared against those of the SLA and the Force-Release simulations of the *discrete-crushing* model, and (b) the evolution of constant load of precompression during the simulations.
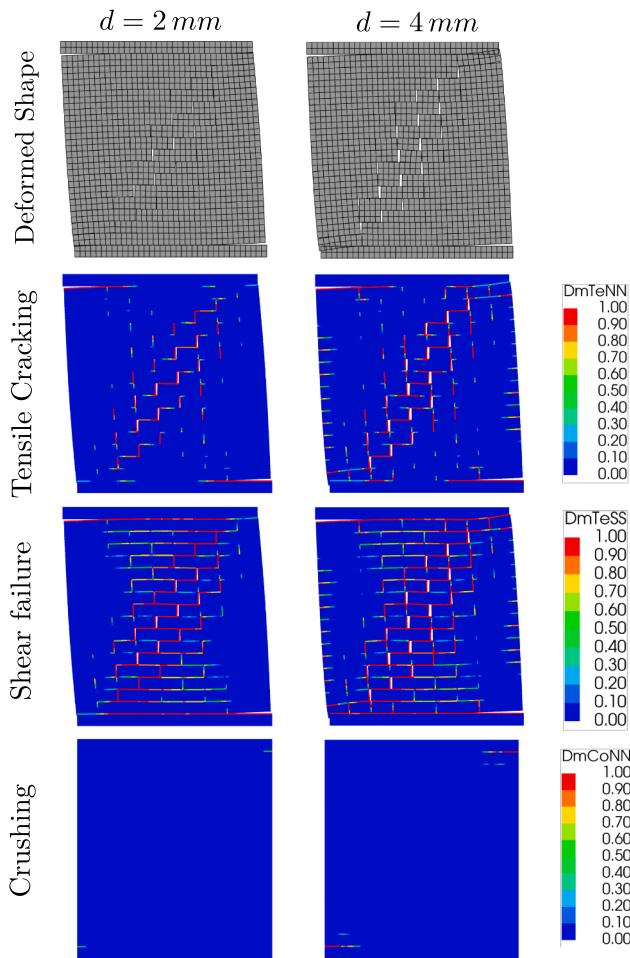

Fig. 13. The deformed profile, and damage plots indicating tensile, shear and crushing failures for the pushover study of reference *discrete-crushing* model, with discrete cracking-shearing-crushing interfaces, using the Force-Release method at 2 mm and 4 mm prescribed lateral displacements.

with multiple cracking zones, SLA may not be appropriate because it does not control a unique damage process zone as in the experiment, and contrarily may incorrectly decrease it due to release of previously applied loads while allowing the structure to relax. Force-Release

method, in this case, may increase the CMOD due to the redistribution. In a quasi-static sequentially linear setup, a truly CMOD controlled experiment with multiple evolving damage zones can be appropriately simulated by the so-called *general* method [11]. For a detailed analysis on the applicability of the approaches, the reader is referred to References [27,38].

Case 3: Crushing in Interfaces vs Continuum. The final variation in this 2D study using SLA (and additionally, the Force-Release method) is that of the *smeared-crushing* model that allows for compressive failure in the continuum elements instead of the interfaces as in the reference *discrete-crushing* model. This is done using the 2D orthogonal fixed smeared crush model with a simple bi-axial Rankine-type failure criterion for crush initiation in the continuum. The nonlinearity parameters for all elements are the same as those in Table 2, except that the continuum elements are provided the crushing parameters. Uniaxial parabolic hardening–softening curves, as in Fig. 3(c), are used but with the band width ripple, for both directions of the 2D crush set-up. The crushing is smeared over a bandwidth of $\sim$ 40 mm and the shear retention function is kept damage-based [36].

The force displacement evolution for the SLA pushover study using the *smeared-crushing* model is as shown in Fig. 14(a). The damage initiation with flexural failure, followed by the diagonal stepped cracks culminating in the toe crushing, as observed in the experiments and in the *discrete-crushing* model are captured well by the *smeared-crushing* model as well, refer Fig. 15. The evolution of the constant overburden load through the analysis is shown in Fig. 16 alongside a Force-Release simulation of the same model for comparison. Due to the good agreement with the Force-Release simulation, only the SLA results are deliberated hereon.

The most noteworthy difference is that the post-peak response involving crushing of the toe is slightly more ductile in the case of the *smeared-crushing* model. To understand this, the evolution of eccentricity of the effective vertical reaction force with respect to the imposed displacement is analysed. The response of both models match up until an imposed displacement of around 2.5 mm, refer Fig. 14. Beyond this point, the inward motion of crushing zone towards the center of the wall is more drastic in case of the *discrete-crushing* model, denoted by parameter β in Fig. 14(b), which indicates complete crushing of the left most part of the toe (roughly half a brick length - Fig. 8). In accordance with Eq. (17), complete crushing also leads to total loss of shear stiffness in this toe region which results in the sliding out of the brick (Fig. 8). The crush zone thus effectively moves more inwards leading to an earlier collapse. However, in case of the *smeared-crushing* model, the smearing out of crushing into the continuum results in a more diffused damage
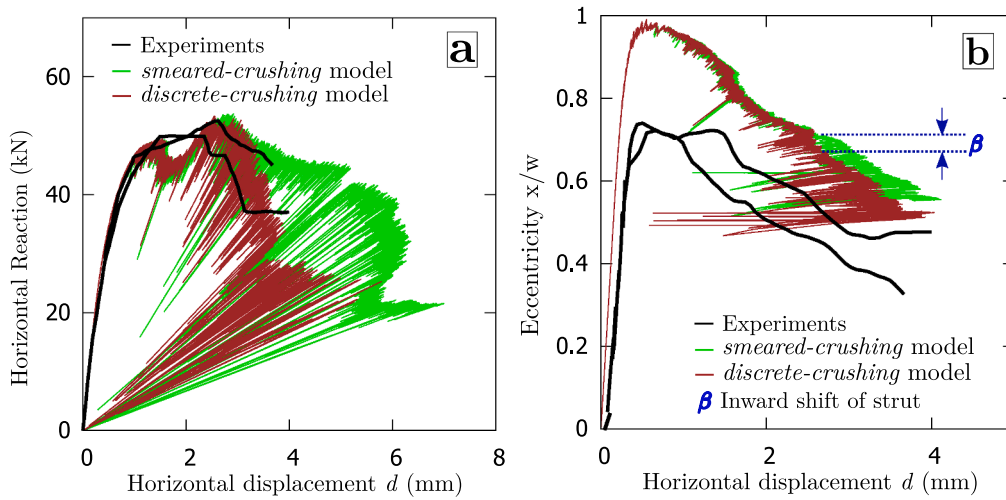
Fig. 14. (a) SLA simulations of the *discrete-crushing* model, and the *smeared-crushing* model with compression nonlinearity smeared into the continuum, and (b) evolution of eccentricity of vertical reaction forces up to 4 mm horizontal displacement.
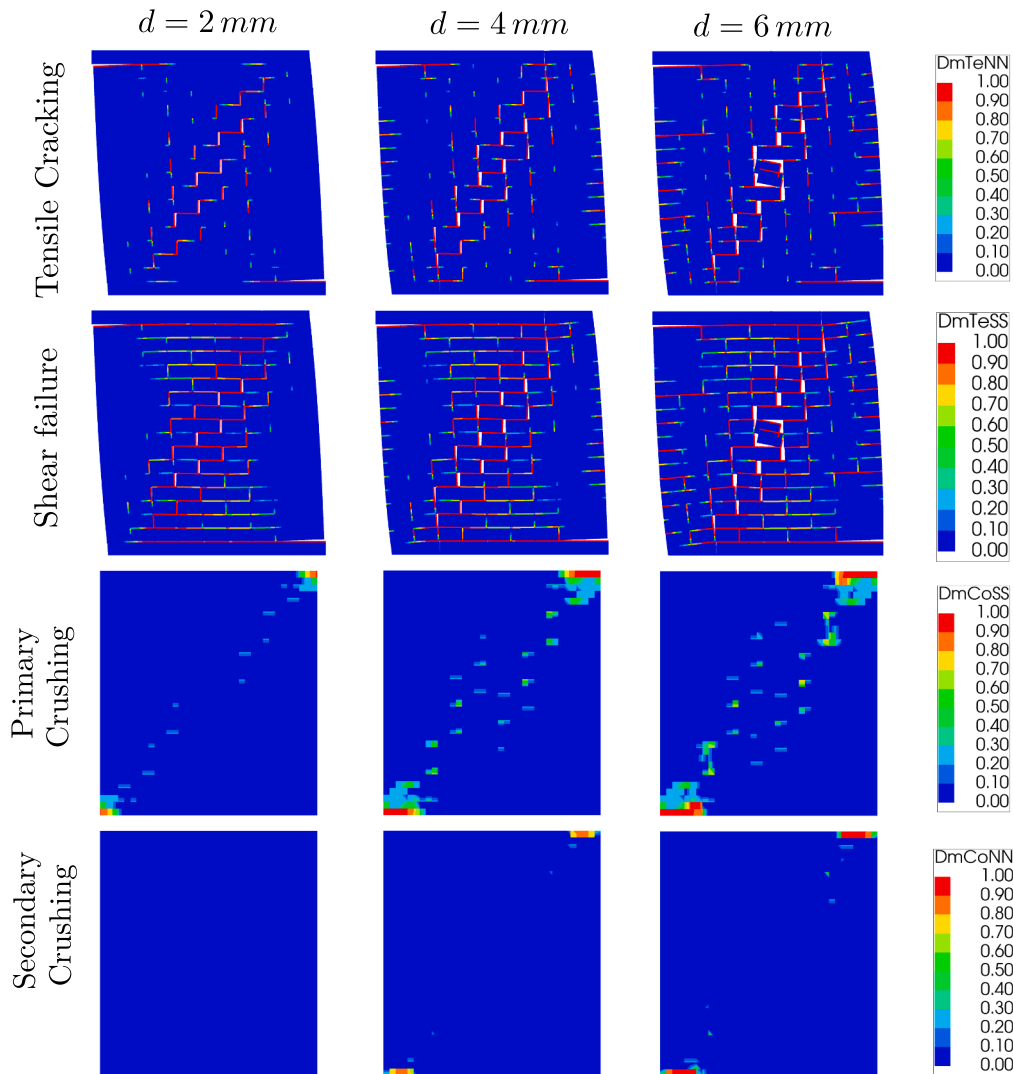

Fig. 15. Damage plots indicating tensile, shear and crushing failures for the pushover study of the *smeared-crushing* model, with discrete cracking and shearing in interfaces while crushing is smeared in the continuum, using SLA at 2 mm, 4 mm and 6 mm prescribed lateral displacements.
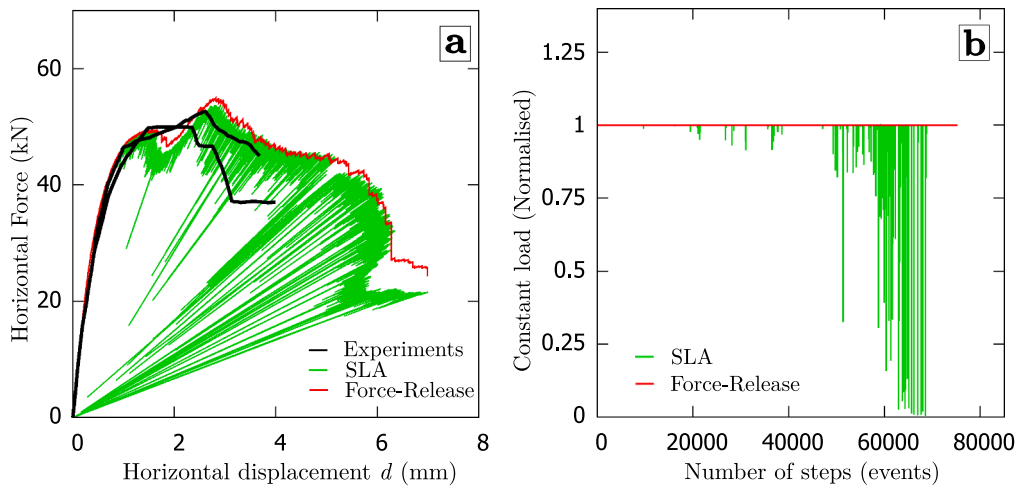
Fig. 16. Force–displacement curves of SLA and the Force-Release simulations of the *smeared-crushing* model, and (b) the evolution of constant load of precompression during the simulations.
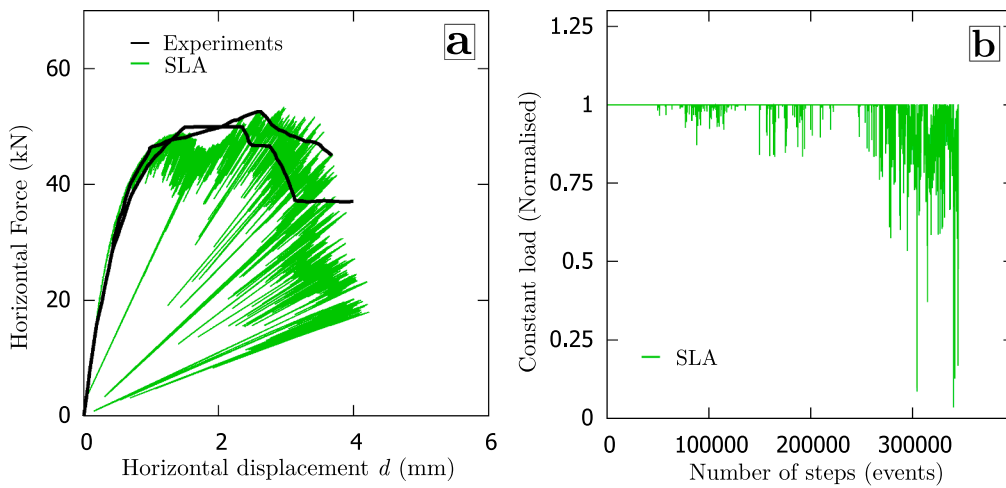

Fig. 17. Force–displacement curves of the experiments compared against those of the SLA for the 3D model, and (b) the evolution of constant load of precompression during the SLA simulation.

zone near the toe region as seen in the plots of Fig. 15. This damage distribution helps delay the inward movement of the crush zone which is decisive for the onset of collapse. That aside, the damage is distinguished

into primary and secondary crushing along the directions of the orthogonal fixed crush-coordinate system of an integration point, which is known to have locking issues, despite the use of a shear retention
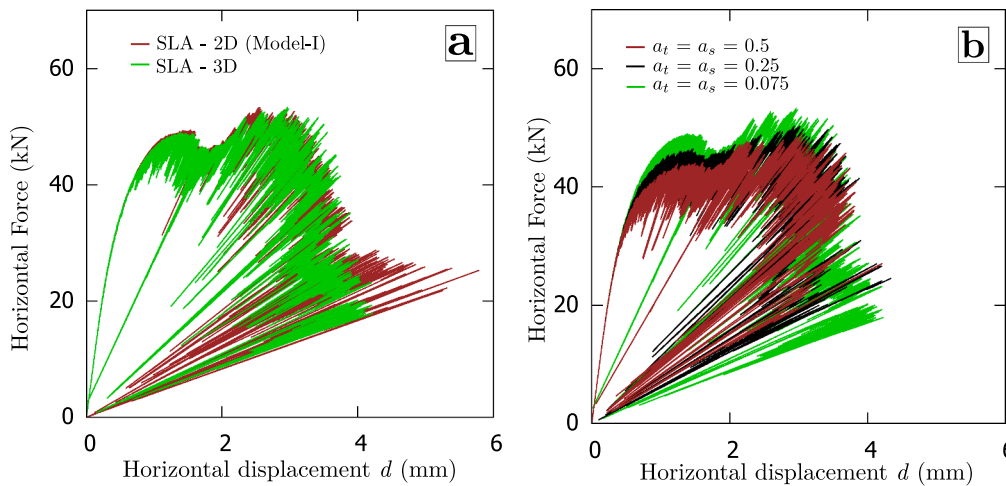

Fig. 18. Force–displacement curves of the 2D and 3D SLA simulations, (b) 3D SLA simulations for varying values of user-specified shear displacement increment factors a_t and a_s.
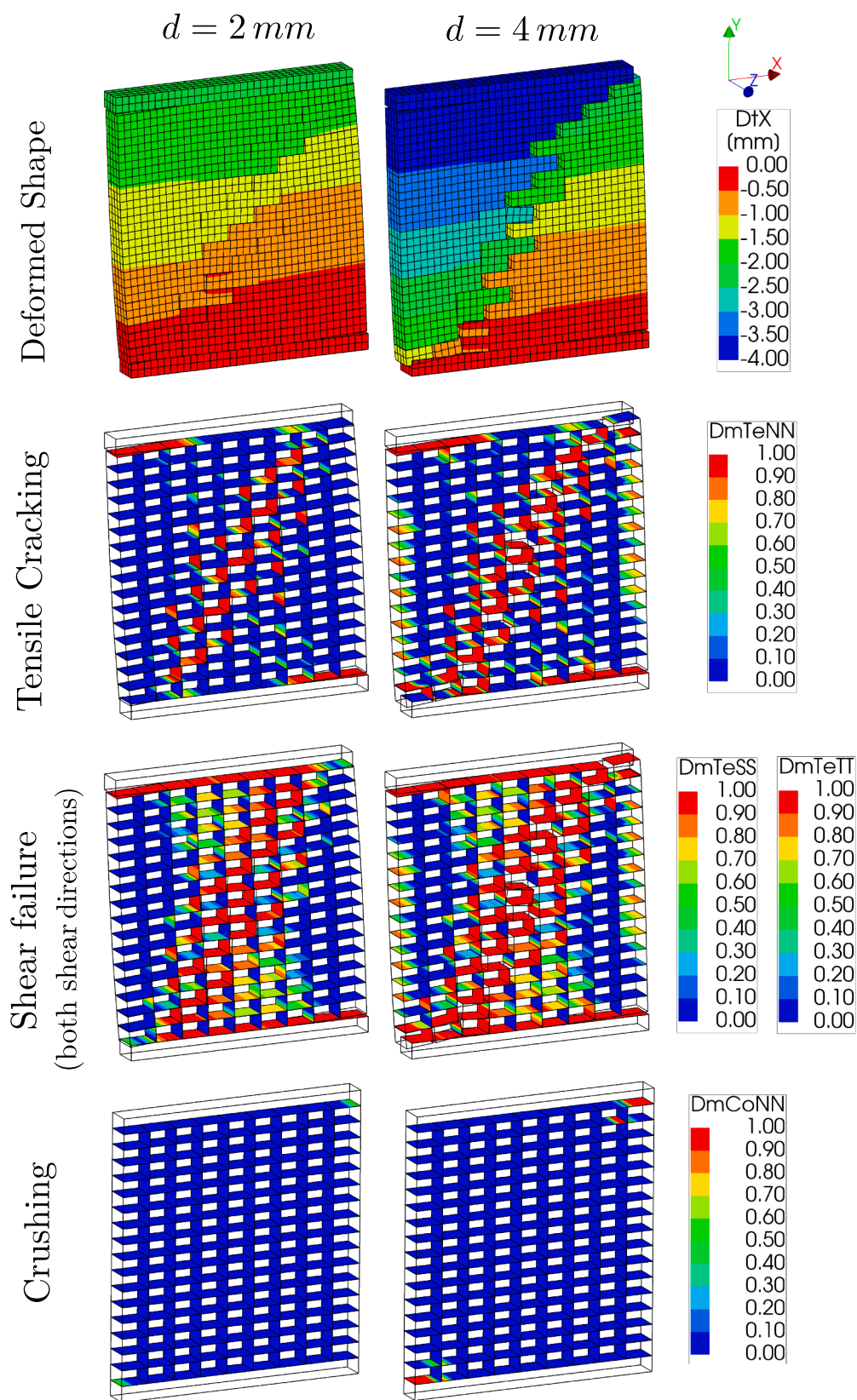
Fig. 19. Deformed profiles, and damage plots indicating tensile, shear and crushing failures for the pushover study of 3D Model using SLA at 2 mm and 4 mm prescribed lateral displacements.

function. There is also some amount of crushing at several locations along the diagonal, due to contact between bricks, which is not observed in the *discrete-crushing* model. The combined effect of these differences results in the slightly more ductile response of the *smeared-crushing* model.

In conclusion, the relatively quicker inward displacement of the crush zone, due to the movement and rotation of the struts, sets off the global softening faster in the case of the reference *discrete-crushing* model as against the *smeared-crushing* model. The ductile response of the latter can be attributed to the larger diffused crush zone coupled with stress locking, which leads to the slower inward propagation of the crush zone, and also more inwards than in the case of the former.

4.2. 3D planar interface micro-model

Finite Element Model. The 3D model of the case study presented thus far is made in the same manner as the 2D model, with regard to the micro-modelling approach, and is therefore not depicted here owing to triviality. The differences are summarised as follows. The mortar joints and the brick–mortar interfaces are lumped together into zero-thickness $4 + 4$ noded planar interfaces with a 2×2 Newton–Cotes integration scheme. The extended bricks are modelled using 8 noded iso-parametric solid elements, all approximately $27.5\ \text{mm} \times 27.5\ \text{mm} \times 27.5\ \text{mm}$ in size, with linear interpolation shape functions and a $2 \times 2 \times 2$ Gaussian integration scheme. All DOFs along the bottom faces of wall are fully constrained, while the top face is prevented against any rotation. The nodes along the top face of the wall are given an initial vertical displacement 0.083 mm, which is the imposed displacement equivalent to an overburden pressure of $0.30\ \text{N/mm}^2$. Subsequently, a lateral displacement is imposed on the top edge to simulate the lateral load. The presented planar interface composite interface formulation is the adopted constitutive model, and all head and bed joints are lumped with the nonlinearities of tensile cracking, crushing and shearing, with material parameters as shown in Tables 1,2. However, for the decoupled Coulomb friction failure mode, user specified discretisation factor of $a_t = 0.075$ and $a_s = 0.075$ for the specified relative shear displacement along the two shear directions, as in Eq. (22), are used as against $a_t = 0.05$ in the 2D analysis. Also, all saw-teeth discretisation factors for tensile and compressive ripple band relations are set to 0.2 whereas narrower ripple bands were used in the 2D analysis. The above mentioned changes in discretisation factors are made to avoid long computational times.

Results & Discussion. Firstly, the SLA simulation of the 3D micro-model shows good qualitative agreement with the the 2D simulation of the reference *discrete-crushing* model (Fig. 18(a)), and the experimental responses of walls J4D and J5D as well (Fig. 17), both in terms of the peak loads and the global softening behaviour that leads to loss of lateral capacity. The deformed profile and damage propagation in the masonry are summarised for the SLA simulation of the 3D Model in Fig. 19 at 2 mm and 4 mm prescribed lateral top displacement d. The damage plots DmTeNN and DmCoNN indicate loss of normal stiffness due to cracking and crushing respectively. The DmTeSS and DmTeTT plots indicate loss of shear stiffness along the two shear directions, which are either due to sliding failures or the damaged based shear reduction due to the associated normal cracking/crushing. All damage plots herein range from 0 to 1 which refer to undamaged and fully damaged cases for the corresponding failure criteria.

Similar to the 2D response, the wall firstly exhibits flexural failure which is visible as horizontal cracks along bed joints at the bottom-right and top-left corners of the wall. After the flexural cracks are fully developed, compressive strut action results in a staggered diagonal shear crack. This damage propagation includes both sliding failure along the bed joints, resulting in loss of both shear stiffnesses, and tensile cracking along head joints, resulting in loss of both normal and shear stiffnesses as is observed in the plots of Fig. 19. Although minor out-of-plane effects

were seen along the staggered diagonal crack and also at the top edge of the wall, they are negligible. The case study, in principle, serves as a good starting case for 3D sliding problems and the proposed formulation shows good promise. Since the 2D formulation has been shown to work equally well with both SLA and Force-Release methods, 3D formulation is shown here only with SLA although the Force-Release simulation should be possible in principle.

One key aspect of simulating sliding problems using SLA is the effect of the user-specified shear displacement increment factors a_t or a_s (Eq. (22)) on the shear capacity. It is most likely that only one of the two has a substantial influence in the present case study since shearing will be dominant in only one direction. However, it is possible in principle to change them both simultaneously. Furthermore, it was noted previously that the curves become less smooth upon increasing values of these factors, but that the peak capacity and post-peak behavior were convergent for moderately large values [8]. However, it is found in a sensitivity study for these factors that the effect is important for sliding problems. It is clear from Fig. 18(b), that values such as $a_t = a_s = 0.5$ or 0.25 result in quicker loss of the mobilised cohesion and lower dissipation of energy. This is because the update in stiffness is rather drastic leading to larger plastic shear displacements than based on the prediction as in Eq. (22), and it is therefore recommended to use this factor appropriately.

5. Concluding remarks

This article proposes a discretised multi-surface failure model for interfaces, enabling cracking, crushing and shearing failure possibilities typical of mechanisms in masonry. This makes it possible to analyse masonry components using sequentially linear methods, in combination with the micro-modelling approach, until full collapse in a robust manner. The constitutive model is presented for both line (2D) and planar interfaces (3D) with regard to determining critical load multiplier and the mode of stiffness update. The model is summarised as follows:

- Shear failure is described by the uncoupled Coulomb friction formulation, allowing for cohesion softening, and updating the shear stiffness based on *specified* shear relative displacement increments.
- Discrete cracking is initiated by a tension cut-off criterion coupled with a uniaxial tension softening saw-tooth law.
- Crushing is initiated by a compression cut-off criterion coupled with a hardening–softening saw-tooth law.

The formulations are then validated using a benchmark study of a pushover analysis on a solid clay brick masonry wall. The wall is first subject to precompression followed by an imposed monotonic lateral displacement, resulting in a diagonal shear failure typical of squat masonry walls. This benchmark is simulated using both 2D and 3D models, and the results of both compare well to the experiments. Firstly, the agreement between the SLA simulation and the experiment is good with regard to the force–displacement relation and the damage patterns. Toe crushing is captured adequately which leads up to the inward movement of the crush zone, in turn due to the inward movement and rotation of two parallel struts, and results eventually in a brittle failure. Secondly, the non-proportional loading strategy used in SLA works well for the presented case leading up to true-collapse. The constitutive formulation works adequately in combination with the incremental Force-Release method as well. Furthermore, the lack of dilatancy in the Coulomb friction formulation does not seem to affect the force displacement relations, although the development of vertical reaction forces are adrift of those from the experiment, both in magnitude and in terms of eccentricity. Nevertheless, there is scope to improve the performance of the proposed composite interface formulation, for e.g. by using a compression criterion as in the traditional elliptical cap model proposed by Lourenco [3,4].

With regard to the sequentially linear approach in general, several

extensions can still be made to extend its applicability mainly in relation to loading or stress history related nonlinear problems. Firstly, the approach is currently being used for monotonic applications. Cyclic loading studies are possible in an incremental approach with non-secant saw-tooth laws [38], and also additionally require a stress-reversal algorithm [39,38], but these are yet to be investigated. Secondly, the approach needs to be extended to large-deformation applications i.e for geometric nonlinear cases. Thirdly, the suitability of the incremental sequentially linear approaches for plasticity based problems needs to be further explored.

CRediT authorship contribution statement

M. Pari: Conceptualization, Methodology, Software, Validation, Investigation, Writing - original draft, Visualization. **A.V. Van de Graaf:** Methodology, Writing - review & editing. **M.A.N. Hendriks:** Writing - review & editing, Supervision. **J.G. Rots:** Conceptualization, Review & Editing, Supervision, Funding acquisition.

Declaration of Competing Interest

The authors declare that they have no known competing financial interests or personal relationships that could have appeared to influence the work reported in this paper.

Acknowledgments

References

[1] Lourenço PB, Milani G, Tralli A, Zucchini A. Analysis of masonry structures: review of and recent trends in homogenization techniques. Can J Civil Eng: Special Issue Masonry 2007;34(11):1443–57. https://doi.org/10.1139/L07-097.

[2] CUR. Structural masonry: an experimental/numerical basis for practical design rules (English version), Tech. Rep. 171, Dutch Version (1994), J.G. Rots (Ed.); 1997.

[3] Lourenço PB. Computational strategies for masonry structures. Ph.D. thesis. Delft University of Technology; 1996.

[4] Lourenço PB, Rots JG. Multisurface interface model for analysis of masonry structures. J Eng Mech 1997;123(7):660–8.

[5] Giambanco G, Rizzo S, Spallino R. Numerical analysis of masonry structures via interface models. Comput Methods Appl Mech Eng 2001;190(49):6493–511. https://doi.org/10.1016/S0045-7825(01)00225-0.

[6] Chaimoon K, Attard MM. Modeling of unreinforced masonry walls under shear and compression. Eng Struct 2007;29(9):2056–68. https://doi.org/10.1016/j.engstruct.2006.10.019.

[7] DeJong MJ, Hendriks MAN, Rots JG. Sequentially linear analysis of fracture under non-proportional loading. Eng Fract Mech 2008;75(18):5042–56. https://doi.org/10.1016/j.engfracmech.2008.07.003.

[8] Van de Graaf AV. Sequentially linear analysis for simulating brittle failure. Ph.D. thesis. Delft University of Technology; 2017. doi:10.4233/uuid:dd9ea945-136c-4b74-bae2-f1a8cf9a6ed9.

[9] Alfaiate J, Sluys LJ. On the use of non-iterative methods in cohesive fracture. Int J Fract 2018;210(1–2):167–86. https://doi.org/10.1007/s10704-018-0270-2.

[10] Eliáš J, Frantík P, Vořechovský M. Improved sequentially linear solution procedure. Eng Fract Mech 2010;77(12):2263–76. https://doi.org/10.1016/j.engfracmech.2010.05.018.

[11] Eliáš J. Generalization of load–unload and force-release sequentially linear methods. Int J Damage Mech 2015;24(2):279–93. https://doi.org/10.1177/1056789514531001.

[12] Graça-E-Costa R, Alfaiate J, Dias-Da-Costa D, Neto P, Sluys LJ. Generalisation of non-iterative methods for the modelling of structures under non-proportional loading. Int J Fract 2013;182(1):21–38. https://doi.org/10.1007/s10704-013-9851-2.

[13] Rots JG. Sequentially linear continuum model for concrete fracture. Proc Fract Mech Concrete Struct (FraMCoS) 2001;2:831–40.

[14] Rots JG, Invernizzi S. Regularized sequentially linear saw-tooth softening model. Int J Numer Anal Meth Geomech 2004;28(7–8):821–56. https://doi.org/10.1002/nag.371.

[15] Rots JG, Belletti B, Invernizzi S. Robust modeling of RC structures with an "event-by-event" strategy. Eng Fract Mech 2008;75(3–4):590–614. https://doi.org/10.1016/j.engfracmech.2007.03.027.

[16] Giardina G, Van de Graaf AV, Hendriks MAN, Rots JG, Marini A. Numerical analysis of a masonry facade subject to tunnelling-induced settlements. Eng Struct 2013;54:234–47. https://doi.org/10.1016/j.engstruct.2013.03.055.

[17] Invernizzi S, Trovato D, Hendriks MAN, Van de Graaf AV. Sequentially linear modelling of local snap-back in extremely brittle structures. Eng Struct 2011;33(5): 1617–25. https://doi.org/10.1016/j.engstruct.2011.01.031.

[18] Pari M, Rots JG, Hendriks MAN. Non-proportional loading for 3-D stress situations in Sequentially Linear Analysis. In: Meschke G, et al. Computational modelling of concrete structures. CRC Press; 2018. p. 931–40. https://doi.org/10.1201/9781315182964-108.

[19] Pari M, Hendriks MAN, Rots JG. Non-proportional loading in sequentially linear analysis for 3D stress states. Int J Numer Meth Eng 2019;119(6):506–31. https://doi.org/10.1002/nme.6060.

[20] Van de Graaf AV, Hendriks MAN, Rots JG. A discrete cracking model for sequentially linear analysis. In: Nenad Bicanic et al., editor, Computational modelling of concrete structures; EURO-C; 2010. p. 409–18.

[21] Ensink SWH, van de Graaf AV, Slobbe AT, Hendriks MAN, den Uijl JA, Rots JG. Modelling of bond behaviour by means of sequentially linear analysis and concrete-to-steel interface elements, in. In: Proceedings of the fourth bond in concrete conference; 2012.

[22] Hendriks MAN, Rots JG. Simulation of creep induced cracking based on sequentially linear analysis. In: Tanabe T, et al., Proc. of the 8th international conference on creep, shrinkage and durability mechanics of concrete and concrete structures; 2009. p. 579–85.

[23] Pari M, Swart W, Van Gijzen MB, Hendriks MAN, Rots JG. Two solution strategies to improve the computational performance of sequentially linear analysis for quasi-brittle structures. Int J Numer Meth Eng 2020;121(10):2128–46. https://doi.org/10.1002/nme.6302.

[24] Georgioudakis M, Stefanou G, Papadrakakis M. Stochastic failure analysis of structures with softening materials. Eng Struct 2014;61:13–21. https://doi.org/10.1016/j.engstruct.2014.01.002.

[25] Slobbe AT. Propagation and band width of smeared cracks, Ph.D. thesis, Delft University of Technology; 2014. https://doi.org/10.4233/uuid:dd9ea945-136c-4b74-bae2-f1a8cf9a6ed9.

[26] Al-Sabah AS, Laefer DF. Meshfree sequentially linear analysis of concrete. J Comput Civil Eng 2016;30(2):04015009. https://doi.org/10.1061/(ASCE)CP.1943-5487.0000474.

[27] Pari M, Hendriks MAN, Rots JG. Non-proportional loading in sequentially linear solution procedures for quasi-brittle fracture: A comparison and perspective on the mechanism of stress redistribution. Eng Fract Mech 2020;230:106960. https://doi.org/10.1016/j.engfracmech.2020.106960.

[28] Liu JX, Sayed TE. On the load-unload (l-u) and force-release (f-r) algorithms for simulating brittle fracture processes via lattice models. Int J Damage Mech 2012;21(7):960–88. https://doi.org/10.1177/1056789514424585.

[29] Feenstra PH. Computational aspects of biaxial stress in plain and reinforced concrete. Ph.D. thesis. Delft University of Technology; 1993.

[30] Ferreira D. Diana user manual, Tech. Rep. Release 10.3, DIANA FEA B.V.; 2019.

[31] van Zijl GPAG, Rots JG, Vermeltfoort AT. Modelling shear-compression in masonry, in. In: Proceedings of the 9th Canadian masonry symposium; 2001.

[32] van Zijl GPAG. Modeling masonry shear-compression: Role of dilatancy highlighted. J Eng Mech 2004;130(11):1289–96. https://doi.org/10.1061/(ASCE)0733-9399(2004)130:11(1289).

[33] van Zijl GPAG. Computational modelling of masonry creep and shrinkage. Ph.D. thesis. Delft University of Technology; 2000.

[34] Raijmakers T, Vermeltfoort AT. Deformation controlled tests in masonry shear walls, Report B-92-1156, TNO-Bouw, Delft.

[35] Raijmakers T, Vermeltfoort AT. Deformation controlled tests in masonry shear walls: Part 2, Report TUE/BKO/93.08, Eindhoven university of technology.

[36] Slobbe AT, Hendriks MAN, Rots JG. Sequentially linear analysis of shear critical reinforced concrete beams without shear reinforcement. Finite Elem Anal Des 2012;50:108–24. https://doi.org/10.1016/j.finel.2011.09.002.

[37] Rots JG, Invernizzi S, Belletti B. Saw-tooth softening/stiffening-a stable computational procedure for rc structures. Comput Concrete 2006;3(4):213–33.

[38] Pari M. Simulating quasi-brittle failure in structures using sequentially linear methods: Studies on non-proportional loading, constitutive modelling, and computational efficiency. Ph.D. thesis. Delft University of Technology; 2020. https://doi.org/10.4233/uuid:ca17d04d-4c40-4856-97cd-8808ac641007.

[39] Eliáš J, Stang H. Lattice modeling of aggregate interlocking in concrete. Int J Fract 2012;175(1):1–11. https://doi.org/10.1007/s10704-012-9677-3.